Food & Function

ROYAL SOCIETY OF CHEMISTRY

PAPER

View Article Online
View Journal | View Issue

Cite this: *Food Funct.*, 2024, **15**, 1627

Effect of beta glucan coating on controlled release, bioaccessibility, and absorption of β-carotene from loaded liposomes†

Taskeen Niaz * and Alan Mackie *

Recently, the use of biopolymers as coating material to stabilise phospholipid-based nanocarriers has increased. One such class of biopolymers is the dietary fibre beta-glucan (βG). In this study, we developed and characterized beta-carotene (βC) loaded βG coated nanoliposomes (GNLs) to investigate the effect of βG coating on the stability, controlled release, bioaccessibility, diffusion and subsequent absorption of the lipophilic active agent. The size, charge (*Z*-potential), and FTIR spectra were measured to determine the physicochemical stability of GNLs. βG coating reduced the bioaccessibility, provided prolonged release and improved the antioxidant activity of the nanoliposomes. Multiple particle tracking (MPT) data suggested that βC-GNLs were less diffusive in porcine intestinal mucus (PIM). Additionally, the microviscosity of the PIM treated with GNLs was observed to be higher (0.04744 ± 0.00865 Pa s) than the PIM incubated with uncoated NLs (0.015 ± 0.0004 Pa s). An *Ex vivo* experiment was performed on mouse jejunum to measure the absorption of beta-carotene from coated (βC-GNLs) and uncoated nanoliposomes (βC-NLs). Data showed that after 2 hours, 27.7 ± 1.3 ng mL^{-1} of βC encapsulated in GNLs and 61.54 ± 3 ng mL^{-1} of the βC encapsulated in uncoated NLs was absorbed by mouse intestinal mucosa. These results highlight that coating with βG stabilise NLs during gastrointestinal digestion and provides more sustained release of βC from nanoliposomes.

Received 26th September 2023,
Accepted 22nd December 2023

DOI: 10.1039/d3fo04123a

rsc.li/food-function

1. Introduction

Delivery of bioactive components from foodstuffs can be challenging, with low absorption and low bioavailability because of poor chemical stability and solubility in the human gastrointestinal tract (GIT).[1] The introduction of nanotechnology to the food industry provides solutions to deal with the challenges and technological barriers associated with solubility, intestinal absorption, and bioavailability of nutraceuticals. Various nano-delivery systems (NDS) have been developed to enhance digestion, control release and absorption of bioactive compounds necessary for human metabolism as well as to avoid nutritional deficiencies.[2] Liposomes are one of the most widely used nanosystems in food research to increase the bioavailability of bioactive compounds. Due to the amphiphilic nature liposomes have the ability to encapsulate both lipophilic and hydrophilic compounds, moreover use of natural readily abundant phospholipids *i.e.*, soy-lecithin in the production of liposomes make it a biocompatible and cost effective nanocarrier for food applications.[3] There have been many investigations of bioactive compounds (vitamins, antioxidants, antimicrobials) encapsulated in nanoliposomes for use in food products.[4,5] These studies have shown that encapsulation of bioactive compounds in nanoliposomes provides long-term safety and stability to different food products *i.e.*, tofu, cheese, yogurt, and meat.[6–9] In a similar study, Marsanasco *et al.* concluded that vitamins E and C encapsulation in a liposomal NDS maintained the heat stability and the activity of these vitamins without modifying the sensory properties of orange juice.[10]

Many challenges are associated with liposomes as oral nanodelivery systems including low resistance to gastric enzymes and pH as well as possible interaction with bile salt in the intestine make NLs unstable, which leads to off-target and burst release of the encapsulated active agent.[11] Oral stability of the liposomes can be improved by surface modifications and coating with polysaccharide polymers[12–17] and it was observed previously that the polymer coatings can not only improve the physicochemical properties but also improve the fusogenic and controlled release properties of the liposomes.[18]

One such polysaccharide is oat β-glucan (βG), which is an FDA (US Food and Drug Administration) approved dietary fibre (DF) with Generally Recognized as Safe (GRAS) status. In 2011, European Food Safety Authority (EFSA) published a study on various DF including βG and the claimed numerous health

Food Colloids and Bioprocessing Group, School of Food Science and Nutrition, University of Leeds, Leeds LS2 9JT, UK. E-mail: a.r.mackie@leeds.ac.uk

† Electronic supplementary information (ESI) available. See DOI: https://doi.org/10.1039/d3fo04123a

benefits associated with DF consumption.[19] In particular, proven health benefits are glucose and cholesterol lowering effect, which reduce the risk of type II diabetes and cardiovascular disease[20–22] by reducing serum low-density lipoprotein (LDL)-cholesterol, improving glycaemic response and modulation of gut microbiota.[23,24] Cholesterol and plasma glucose lowering effect of βG is also associated with the increase in the viscosity of chyme, which affects gastrointestinal motility and hydrolysis rate in the GIT.[25]

In addition to the higher viscosity effect in the upper GIT, βG may also alter the microviscosity of the mucus layer in the small intestine, hence decreasing its permeability by increasing overall polymer concentrations and decreasing porocity.[26] Additionally, sequestering of bile acids, by entrapment of mixed micelles and decrease in enterohepatic bile circulation by forming a complex between bile salt micelles and βG are the other suggested mechanisms behind low absorption of lipophilic compounds in the intestinal lumen.[27] This ability of native β-glucan to slow digestion and metabolism could negatively affect the bioaccessibility and absorption of beneficial bioactive compounds. However, in a study by Shah *et al.*, it was suggested that βG is an excellent coating material for nano-delivery of nutraceuticals and can exhibit enhanced anti-obesity and antioxidant activity.[28] Similarly, Xiao *et al.* discussed the antiobesity, cholesterol lowering and antihypertensive effects of beta-glucan by inhibiting α-Amylase, α-Glucosidase, lipase, and angiotensin-converting enzymes activity.[29] These studies also discussed the potential biomedical application of beta glucan-based NDS and the control release properties of these nanoparticles into food systems.[30–33]

Beta carotene (βC) was used as a model bioactive compound in this study because of its well-known biological activities like antioxidant activity, anticancer, and provitamin A activity.[17] On the other hand, low stability and poor bioaccessibility and bioavailability due to its hydrophobic nature[34] make beta carotene an excellent choice for nanoencapsulation. To the best of our knowledge, no study has been done yet on the DF *i.e.*, βG based NDS diffusion through mucus, effect on mucus microviscosity and subsequent absorption in intestinal epithelial cells. Therefore, in this study, we developed a novel nano-delivery system (NDS) by coating nanoliposomes (NLs) with βG and investigated the bioaccessibility & controlled release properties of these NDS, their diffusion through the mucus membrane followed by the absorption *via* intestinal epithelial cells after gastrointestinal digestion.

2. Materials and methods

2.1 Materials

High viscosity oat beta-glucan was purchased from Megazyme/Neogen (UK). Beta-carotene, soy phospholipids, tripolyphosphate (TPP), phosphate buffered saline (PBS), D-glucose and mannitol were purchased from Oxoid-Thermo Fisher scientific, UK. Different digestive enzymes such as pepsin (P7000-25G, actual activity: 474 U mg^{-1}), pancreatin (P7545, trypsin activity 4000 U U), bovine bile (B8631-100G), sodium taurocholate and pefabloc were provided by Sigma-Aldrich (UK). Salts to prepare digestive buffers *i.e.*, sodium bicarbonate, sodium chloride, potassium and magnesium chloride and potassium dihydrogen sulphate were also provide by Sigma-Aldrich (UK). Guanidine hydrochloride, EDTA, *N*-ethylmaleimide, sodium azide, sodium phosphate dibasic, sodium dihydrogen phosphate/monobasic, sodium phosphate and Nile red were obtained from VWR international.

2.2 Methods

2.2.1 Fabrication and characterization of β-glucan-nanoliposomes (GNLs). nanoliposomes (NLs) were prepared by thin film hydration followed by the extrusion method as described previously with slight modifications.[35] Briefly, 0.5% of soy-lecithin phospholipids (94% phosphatidylcholine and 2% triglycerides) were dissolved in an 80% of methanol solution. The organic solvent was evaporated using Genevac (EZ-2 plus) (Fisher Scientific Ltd, Leicestershire, UK) (25 °C, Method: Very Low BP Mix) to obtain a thin lipid film. The thin film was hydrated by the addition of PBS (10 mM, pH 7.4) followed by 5 freeze-and-thaw cycles with liquid nitrogen. The pH of the solution was adjusted to 5.5 and samples were sonicated using QSonica Sonicator (40% amplitude, 1s on, 2 s off) for 20 min followed by 10 times extrusion through 100 nm polycarbonate membranes with a mini extruder (Avanti polar lipids, Inc., Alabama, USA).

In a second step, β-glucan-nanoliposomes (GNLs) was prepared by dissolving 0.3 g of βG in 100 mL of NaOH (1%, w/v) solution and stirred (600 rpm) for 60 min at 90 °C on a magnetic stirrer. After one hour, the temperature was reduced to 40 °C; pH of the solution was adjusted to 5.5 and stirred for 30 more minutes. GNLs were obtained by the dropwise addition of NLs solution to βG solution (1 : 1 v/v) under stirring for 2 h. Finally, the synthesized GNLs were stabilized by dropwise addition of 0.1% sodium tripolyphosphate (TPP) solution (200 μL mL^{-1}), to crosslink the βG layer and ensuring the integrity of the absorbed layer. The resultant solution was filtered with a 0.24 μm syringe filter and stored for further analysis.

For β-carotene (βC) loaded GNLs (BC-GNLs), 1 mg mL^{-1} of βC was dissolved in 80% methanol solution containing phospholipids before thin lipid film preparation step.

2.2.2 Size and *Z*-potential measurements. The mean particle size (*Z*-average), polydispersity index (PDI) and zeta potential (ZP) of fabricated Nano systems were determined using dynamic light scattering (DLS) as described previously.[36] The samples were diluted in Milli-Q water and measurements were taken at 25 °C using a Malvern DLS Zetasizer Nano ZS (Malvern, United Kingdom) at a scattering angle of 173°.

2.2.3 Encapsulation efficiency of βC-GNLs. The encapsulation efficiency (EE) of βC was determined according to the method previously published[37] with a slight modification. The EE % was quantified by measuring the free βC (not encapsulated) in the supernatant. For this purpose, amount of free βC was extracted using an organic solvent method as follows. The sample was added to an equal amount (1 mL) of *n*-hexane and

then centrifuge at 8000 rpm for 5 min. The process was repeated three times and the supernatant was collected to quantify the βC *via* HPLC as described previously by.[38]

For the quantification of βC by HPLC (Agilent ZORBAX Eclipse XDB), the mobile phase was composed of acetonitrile-dichloromethane (70 : 30, v/v) with flow rate of 1 mL min^{-1} and a C18 column, the column temperature of 35 °C, and sample absorbance was measured at 450 nm. Quantification of samples were performed by comparing sample data with pure standards (βC), prepared at different concentrations in *n*-hexane. Each experiment was performed in triplicate. The EE was calculated as follows.

$$\mathrm{EE}\,\% = \frac{T_{\beta C} - F_{\beta C}}{T_{\beta C}} \times 100$$

where "$T_{\beta C}$" is the total amount of β-carotene added to the nanosystems and "$F_{\beta C}$" is the free amount of β-carotene in the supernatant.

2.2.4 Storage stability. Storage stability of βC-GNLs was accessed at 4 °C (refrigerator storage) and 25 °C (room temperature). The retention rate (RR), size, zeta potential, and PDI analysis were determined after 0, 7, 14, and 30 days of storage in the dark.[39,40] Size, zeta potential (ZP), and PDI analysis were performed as described in section 2.2 and the retention rate of βC was calculated according to the following equation.

$$\mathrm{RR}(\%) = \frac{\text{Encapsulated amount of βC in nanosystems after storage}}{\text{initial amount of βC in nanosystems}} \times 100$$

2.2.5 Fourier transforms infrared (ATR-FTIR) spectroscopy. The infrared spectra of GNLs and βC-GNLs were recorded with ATR-FTIR Spectrophotometer (CARY 630, Agilent Technologies, USA) at room temperature. The spectrum was recorded within the range of 500–4000 cm^{-1}

2.2.6 *In vitro* gastrointestinal tract digestion. *In vitro* simulated GIT digestion was performed to determine the fate, bioaccessibility and absorption of βC loaded glucan coated nanoliposomes.[41] The composition of the salivary, gastric, and intestinal fluids are listed in Table 1. Subsequently the *in vitro* digestion simulation was conducted according to the INFOGEST digestion model[42] as follows.

Oral phase: equal amount of void and loaded GNLs were mixed with 5 mL of simulated salivary fluid (SSF, pH 7) in a 50 mL Falcon tube. Subsequently, 25 μL of 0.3 M $CaCl_2$ and 975 μL of dH_2O were added and the digestion tube was incubated in a shaking incubator (S1900R, Robus Technologies. UK) at 37 °C (80 rpm) for 5 min.

Gastric digestion: in this phase, 6.4 mL of simulated gastric fluid (SGF, pH 3) was mixed with the 10 mL oral bolus. Subsequently, 1.6 mL of pepsin with 474 U mg^{-1} of enzymatic activity, 5 μL (0.3 M) of $CaCl_2$ were added, and the pH of the dispersion was adjusted to 3 using 1 M HCl solution. The solution was incubated in a shaking water bath at 37 °C (80 rpm) for 2 hours.

Small intestine phase: after two hours of gastric digestion, an equal amount of simulated intestinal fluid (SIF, pH 7) was added to the gastric phase. Followed by the addition of 2.5 mL of fresh bile (163.28 mg mL^{-1}), 40 μL of $CaCl_2$ (0.3 M) and 5 mL of pancreatin solution, containing 0.617 g, which is 4000 U of trypsin activity. Finally, the pH was adjusted to 7 with 1 M NaOH solution and the tube was again placed in the shaking water bath at 37 °C (100 rpm) for 2 h. The enzyme activity in all samples was stopped by addition of 0.1M Pefabloc (10 μL for 200 μL of digesta).

2.2.7 *In vitro* release and bioaccessibility β-carotene. The amount of βC released from the coated and uncoated NLs was measured during *in vitro* gastrointestinal digestion. The *in vitro* release profile used 200 μL samples removed at 0, 30 and 60 min of gastric and intestinal digestion. The samples were then centrifuged at 15 000 rpm for 60 min, and the supernatant was collected. Release amount (%) of βC was extracted and quantified according to the method mentioned in section 2.3 and measured as follows

$$\%\text{release of βC} = \frac{\text{Amount of βC in the supernatent}}{\text{Total amount of βC in the sample}} \times 100$$

Bioaccessibility was taken to be the fraction of βC that was solubilized in mixed micelles as described previously.[36] For bioaccessibility measurements, 500 μL samples were collected at the end (120 min) of small intestinal digestion phase and centrifuged at 30 000 rpm (Beckman Coulter, |Avanti centrifuge J-30) at 25 °C for 1 hour. The middle layer containing the micellar phase was collected and filtered *via* a syringe filter. Finally, βC was extracted and quantified according to the

Table 1 Chemical composition of simulated salivary (SSF), gastric (SGF), and intestinal (SIF) fluids (stock solutions) and minimum volumes needed for the preparation of 400 mL of each simulated digestion buffer in 1.25× concentration (working solutions)

Chemical/salts	Stock conc. (g L^{-1})	Stock conc. (M)	SSF (make up to 400 mL) Vol. of stock (mL)	SGF (make up to 400 mL) Vol. of stock (mL)	SIF (make up to 400 mL) Vol. of stock (mL)
KCl	37.3	0.5	15.1	6.9	6.8
KH_2PO_4	68	0.5	3.7	0.9	0.8
$NaHCO_3$	84	1	6.8	12.5	42.5
NaCl	117	2	0	11.8	9.6
$MgCl_2(H_2O)_6$	30.5	0.15	0.5	0.4	1.1
$(NH_4)_2CO_3$	48	0.5	0.06	0.5	0
Adjust the pH			pH 7	pH 3	pH 7

method mentioned in section 2.3 and the bioaccessibility was measured as

$$\text{Bioaccessibility (\%)} = \frac{C_{\text{Micelle}}}{C_{\text{raw digesta}}} \times 100$$

where C_{micelle} and $C_{\text{raw digest}}$ are the concentration of βC in micelle fraction and in collected raw digests after *in vitro* digestion.

2.2.8 Antioxidant activity assay

2.2.8.1 (DPPH radical scavenging assay). To determine the antioxidant activity of beta carotene-loaded NLs and GNLs during each phase of digestion, DPPH radical scavenging assay was performed according to the method mentioned previously.[39,43]

Briefly, 1 mL of undigested and digested (from each phase of digestion) BC-NLs as well as BC-GNLs was mixed with 3 mL of DPPH solution, prepared in ethanol (0.04 mg mL^{-1}). The mixture was kept for 30 min in the dark and then its absorbance was measured at 517 nm.

The DPPH-scavenging activity calculated as follows

$$\text{DPPH}_{\text{scav}}(\%) = \left(1 - \frac{A_s - A_c}{A_k}\right) \times 100$$

here, 'A_s' is the absorbance of samples with DPPH solution 'A_c' is the OD of the samples without DPPH solution (only ethanol) and 'A_k' is the absorbance of DPPH ethanol solution without samples.

2.2.8.2 Folin–ciocalteu assay. Total phenolic content of the beta carotene-loaded NLs and GNLs during each phase of digestion was performed by the FC assay as described in Rumpf *et al.*[44]

For the analysis, 10 μL mL sample solution (free βC, βC-NLs and βC-GNLs) before and after *In vitro* digestion were added into each well of 96 well plate followed by the addition of 40 μl Folin reagent (12.5% in deionised water). One minute after adding the FC reagent, 150 μl of 4% sodium carbonate solution was added in to each well and the plate was incubated for 30 min at 40 °C. After incubation, absorbance was measured at 765 nm on Tecan Spark plate reader. Results expressed as Gallic acid equivalents (GAE) with the following equation

$$\text{GAE}\left(\frac{\mu g^{-1}}{m\,L^{-1}}\right) = \frac{A_{\text{sample}} - I_{\text{cal}}}{S_{\text{cal}}}$$

where A_{sample} is the absorbance of the sample, I_{cal} is the intercept of the calibration curve, and S_{cal} is the slope of the calibration curve. The TPC calculated as follow from GAE and initial concentration of the sample.

$$\text{TPC (\%)} = \frac{\text{GAE}}{C_{\text{initial}}} \times 100$$

2.2.9 Mucus penetration study *in vitro*

2.2.9.1. Collection and purification of porcine intestinal mucus. Porcine intestinal mucus was obtained according to the method previously described by Mackie 2016. Briefly, porcine intestines were collected immediately after slaughter from the animal facility and transported to the lab in crushed ice. Once reached in the laboratory porcine intestine was rinsed with ice-cold phosphate buffer containing protease inhibitor (10 mM phosphate pH 6.5, 5 mM EDTA, 0.5 mM Pefabloc, AEBSF). After rinsing intestine was cut out flat and mucus was gently scraped off from the jejunal surface with a slide. The mucus sample was collected in small aliquots, frozen in liquid nitrogen, and stored at −80 °C for further use.

Extraneous debris (such as cellular debris and digesta) was removed by extracting the mucus overnight at 18–22 °C with gentle (30 rpm) stirring in 7 volumes of extraction buffer (10 mM sodium phosphate, pH 6.5, containing 4 M guanidine hydrochloride, 5 mM EDTA, 5 mM *N*-ethylmaleimide and 0.02% w/v sodium azide). Precipitated material was collected after centrifugation (30 min at 22 000 × g (10 °C)) and re-extracted again with 10 volumes of extraction buffer. The insoluble precipitate (crude mucin) was collected and purified further by Caesium chloride (CsCl) density gradient centrifugation method.[45] Briefly, the crude mucin was diluted with 10 mM sodium phosphate buffer (pH 6.5) containing 6 M guanidine hydrochloride (GuHCl) and adjusted to a density of 1.2 g ml^{-1} with CsCl and centrifuged (55 000 rpm at 10.0 °C for 62 h in Beckman Coulter, |Avanti centrifuge J-30). Aliquots of 0.5 ml were sampled, the absorption at 280 nm was measured, and 2 μL of each fraction was spotted and stained with Alcian blue. UV- and Alcian blue-positive aliquots were pooled and repeat centrifugation as before, preparing 3 different CsCl solutions (1.46, 1.56 and 1.6 g mL^{-1}) in 10 mM phosphate buffer, 0.5 M GuHCl, pH 6.5. Fractionate tube contents, determine density and measure absorbance at 260 and 280 nm as before.

The alcian blue positive fractions were pooled with mucin and dialysed against phosphate buffer to remove CsCl (dialysis tubing of 10 kDa) and stored at 4 °C for further use.

2.2.9.1 Multiple particles tracking and micro-viscosity. To determine the effect of beta glucan-coated nano carrier on the microviscosity of the mucus we performed particle-tracking experiment and the movement of GNLs in porcine intestinal mucus was evaluated.[46–48] To perform this experiment, Nile red (NR) encapsulated NLs and GNLs were prepared similarly to βC loaded nanocarriers. After fabrication, 1 μL of fluorescence-labelled NLs and GNLs were diluted with 10 μL of 25 mM Bis-Tris buffer (pH 6.5, 0.15 M NaCl) containing 7.4 mM Sodium Taurocholate to mimic human bile. Two μL of diluted GNLs were mixed into 40 μL of porcine intestinal mucus, placed in a confocal dish, and left it for half an hour at 37 °C. The movements of GNLs were observed under the 100× oil immersion of the ultra-high resolution LSM880 confocal microscope with a time resolution of 50 ms. The movement of individual particle trajectories were analysed by Image-Pro 10 software. Mean square displacement (MSD) and diffusion coefficient (D_{eff}) were calculated using the following equation:

$$\text{Mean square displacement (MSD)} = \Delta r^2(\Delta t)$$

$$\Delta r^2 = \Delta x^2 + \Delta y^2$$

where Δx and Δy are particle displacements in the 'x' and 'y' directions and 't' represents the time over which the movement of particles was calculated.[48]

Effective diffusivities (diffusion coefficients, D_{eff}) were obtained from

$$D_{eff} = MSD/4\Delta t$$

Then the microviscosity of mucus (η) was calculated using the Stokes–Einstein equation,

$$\eta = \frac{K_B T}{D 6\pi r}$$

where 'D' is the diffusion coefficient independent of time, 'K_B' is Boltzmann's constant, 'T' is an absolute temperature in Kelvin and 'r' is the radius of GNLs.

2.2.10 *Ex vivo* intestinal transport of dietary fiber-coated nanocarriers using rat jejunum. The *ex vivo* intestinal transport study was performed using an Ussing chamber as follow, Gut from 6-week old freshly anesthetized C57BL6 mouse was supplied by animal facility (Central Biomedical Services, University of Leeds, UK). All procedures were approved by the University of Leeds Animal Welfare Ethical Review Board and covered by the appropriate licences (PEL number: XDE639D76) under the UK Home Office Animals Scientific Procedures Act (ASPA) 1986. After removal the internal contents, gut were washed twice with ice-cold Krebs–Ringer bicarbonate (KRB) solution. Followed by immediate immersion of intestine in ice cold ringer solution with 11 mM D-glucose (pH 7.4) and shifted to laboratory. Then, about 2 cm of the intestinal segment were excised from the jejunum part of the intestine followed by the removal of the serosal layer from the tissue. Mount the tissue on a cassette and insert it between the two chambers with the mucosal side of intestinal tissues facings the apical chamber and the serosal side facing the basolateral chamber. One mL of ringer + mannitol solution was added to each side of the chamber and TEER (transepithelial electrical resistance) value was measured constantly throughout the experiment. The intestinal tissues with a TEER value less than 20 Ω cm^2 were considered poorly viable and excluded from the experiment.[49]

For the absorption study, βC loaded NLs and GNLs were subject to digestion (section 2.6). 0.5 mL of digesta was collected at the end of the intestinal phase and added to the apical side of the Ussing chamber. 200uL samples were collected from each chamber after 20, 40, 60, and 120 minutes. βC was extracted from each sample by adding Hexane/ethanol/acetone (50 : 25 : 25, v/v/v) into each sample followed by centrifuge at 15 000*g* for 30 min and quantify with HPLC as mentioned previously in section 2.3. The absorption was expressed as the amount of βC (ng mL^{-1}) in the serosal side of jejunum tissue.[17]

2.2.11 Statistical analysis. All experiments were performed at least three times and data were expressed as the mean ± standard deviation. Results were analysed by one-way ANOVA followed by Tukey and Dunnett test and determined significance ($p < 0.05$ or $p < 0.01$) with 95% confidence interval using Minitab software version 17.

3. Results and discussion

3.1 Evaluation of mean particle size, polydispersity index (PDI) and potential (ZP)

Particle size is a critical parameter, effecting the encapsulation efficiency and release of bioactive compounds in nanosystems. Similarly, Zeta potential and PDI are also important to evaluate the physical stability and biological activity of any NDS. The mean particle size, polydispersity index (PDI) and zeta potential (ZP) of empty and carotenoid-loaded nanoliposomes as well as glucan-coated nanoliposomes are shown in Fig. 1A.

The average size, PDI and ZP of uncoated NLs were 80 ± 2.04 nm, 0.13 and −31.6 mV, respectively. After coating with βG the size of NLs increased from 80 nm to 154.2 nm, which can be attributed to the thickness of the βG coating on the GNLs surface. The ZP changed from −31.6 mV (uncoated NLs) to −47.9 mV (GNLs) with a slight increase in PDI (0.25). A

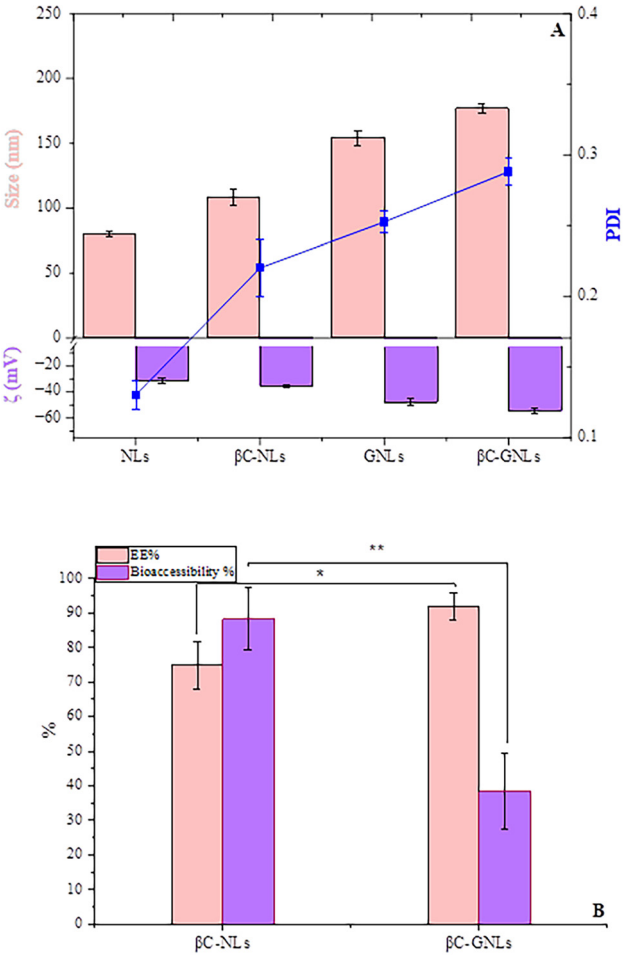

Fig. 1 (A) Dynamic light scattering analysis *i.e.*, size (pink bars), polydispersity index (blue line), and zeta potential (purple bars) of NLs: void liposomes, βC-NLs: beta-carotene loaded liposomes, GNLs: glucan coated liposomes and βC-GNLs: beta-carotene loaded glucan coated liposomes, (B) encapsulation efficiency of coated and uncoated liposomal nanocarriers and *in vitro* bioaccessibility of nano encapsulated βC during gastrointestinal digestion. Values are the means $n = 3 \pm$ SD (**$P < 0.01$, *$P < 0.05$).

slight increase in the magnitude of ZP values of NLs from −31.6 mV to −35.3 mV and −47.9 mV to −54.5 mV in GNLs was observed after βC encapsulation. This could be attributed to the bigger gap between the head group of the phospholipid bilayer after βC encapsulation and to the hydrophobic stabilization of NLs with glucan coating.[50] The ZP value of any nanosystem higher than ±30 mV is considered a stable.[51,52] Therefore, our results here suggest that GNLs are more stable structures than NLs. The negative ZP could be due to the presence of TPP cross-linker (added to stabilize the beta-glucan coatings on nanoliposomes during fabrication).[31] PDI values of all nano-formulations are less than 0.3, which indicates the homogeneous size distribution of fabricated nanosystems.

After encapsulation with βC, the mean particle size of NLs changed from 80 nm to 108 nm. However, no significant change in the particle size of GNLs was observed after βC encapsulation. This suggests that βC is encapsulated in the lipid bilayer of GNLs. Our data is consistent with previous results, where it was suggested that the position and orientation of beta carotene in the lipid bilayer increases the NL diameter.[39] Furthermore, no significant change was observed in ZP values of nanosystems after βC encapsulation owing to its neutral charge. Secondly, it also suggests that almost all of the βC was encapsulated inside and not present on the surface of nanocarriers.

3.2 Encapsulation efficiency (EE%)

The encapsulation efficiency of βC in NLs was about 76.0 ± 3.0% (Fig. 1B). βC due to its hydrophobic nature orients itself deeply within the hydrophobic region of the phospholipid bilayer, therefore can be encapsulated in the NLs at significant concentrations. These results are consistent with a previous study that shows liposomes could encapsulate nonpolar drugs in their membranes, specifically between the phospholipid bilayers dominated by the hydrophobic hydrocarbon chain.[53] However, these interactions are van der Waals or weak noncovalent interactions and allow βC to be released quickly from liposomes.[54] After coating with βG, the EE% increased to 92 ± 6%, this higher EE could be due to the fact that βG coating provided an extra barrier, improved the stability of NLs, and did not allow the entrapped or surface-associated carotenoids in NLs to be released.[55] Hence, resulting in higher EE% in GNLs. Comparable results were observed previously where biopolymeric coating inhibits carotenoid leakage from the nanoliposomes core during the preparation procedure and resulted in higher EE%.[56]

3.3 FTIR

The intermolecular interaction between the beta-glucan coating and core phospholipid-based liposomal vesicles as well as with encapsulated βC was investigated by FTIR (Fig. 2).

In the FTIR spectra of the control NLs (Fig. 2A), characteristic spectral peaks of the phospholipid bilayer appeared at approximately 3310.6 cm^{-1}. This peak represents the O–H stretching vibration of H_2O molecules which are associated with the lipid bilayer *via* H-bonding and is the main characteristic peak for intact liposomal surface.[57] Two small bands at 2938 cm^{-1} and 2848 cm^{-1} represent the symmetric and asymmetric stretching of C–H vibrations belonging to CH_2 groups of alkyl chains and CH_3 terminal groups, respectively. A broad but dull peak at 2109 cm^{-1} corresponds to the stretching vibration of the ester C=O groups of phosphatidylcholine. The broader strong band at 1646 cm^{-1} is related to the stretching vibration of C=C unsaturated aliphatic groups in fatty acid chains.

Additional to these characteristic peaks of liposomes, absorption bands appear at 1215 cm^{-1} and 1120 cm^{-1} representing an asymmetric and symmetric stretch of PO_2^-: a typical representation of phosphate groups in the polar head of NLs. All these major bands associated with the soy phospholipid NLs were also reported in previous studies.[58,59] In the FTIR spectra of pure β-carotene (βC), a sharp peak observed at 966.5 cm^{-1} (represents the Trans C–H conjugated alkene group) is the characteristic peak used to identify βC. In βC-NLs, this characteristic peak can be observed at 1064.4 cm^{-1}, which confirms the presence of βC in the NLs structure (Fig. 2A–I). Additionally, this βC signal is present in the PO_2^- polar head region of the NLs, which confirms βC presence in the hydrophobic regions (lipid bilayer) of the NLs.[60,61] FTIR absorption spectrum of pristine β-glucan (Fig. 2B) consisted of strong and broad absorption bands of the O–H group at 3332 cm^{-1} and C–H stretching vibrations at 2893 cm^{-1}.[62] The absorption peak at 1653 cm^{-1} in the β-glucan spectrum belongs to the glucose ring, and a sharp signal at 1019 cm^{-1} corresponds to the ring vibrations overlapped with stretching vibrations of the C–OH glycosidic bond.[63,64] A small shoulder peak at 903 cm^{-1} represents the β-configuration of the glucan linkage.

In absorption spectrum of GNLs band at 1416 cm^{-1} (Fig. 2B & B-I), represents the two characteristic band regions (1600–1400 cm^{-1}; glucose ring vibrations and 1000–1300 cm^{-1}; stretching vibrations of glycosidic bond between two glucose subunits) of oat βG. The receiving of this signal confirms the presence of glucan polymer layer (glucose unit together with glycosidic bond) on NLs surface. Additionally, in GNLs, the appearance of a large absorption peak at 3321 cm^{-1} reflects the increase in hydrogen bonding.[30,65] This confirms the interaction between the O–H group of βG and the O–H stretching vibration of H_2O molecules, which are associated with the lipid bilayer *via* H-bonding. A peak at 2106 cm^{-1} could be due to the OH–PO stretch, which could be attributed to the linkage between a phosphoric group of TPP and the CH_2OH group of the GNLs. Sharp bending vibrations of bound H_2O molecules can be seen at 1646 cm^{-1} (indicating the presence of moisture) in the coated layer. As stated, above βC owing to its hydrophobic nature reside in the lipid bilayer structure of NLs hence once encapsulated it effect the orientation of PO_2^- polar head region of the NLs and its associated H_2O molecules. Which would affect the H-bonding interaction between βG, and NLs core this effect can be observed in the FTIR spectrum of βC-GNLs where signal shift of H-bonding peak can be observed from 3321 cm^{-1} (in GNLs) to 3295 cm^{-1}. Except slight shift in

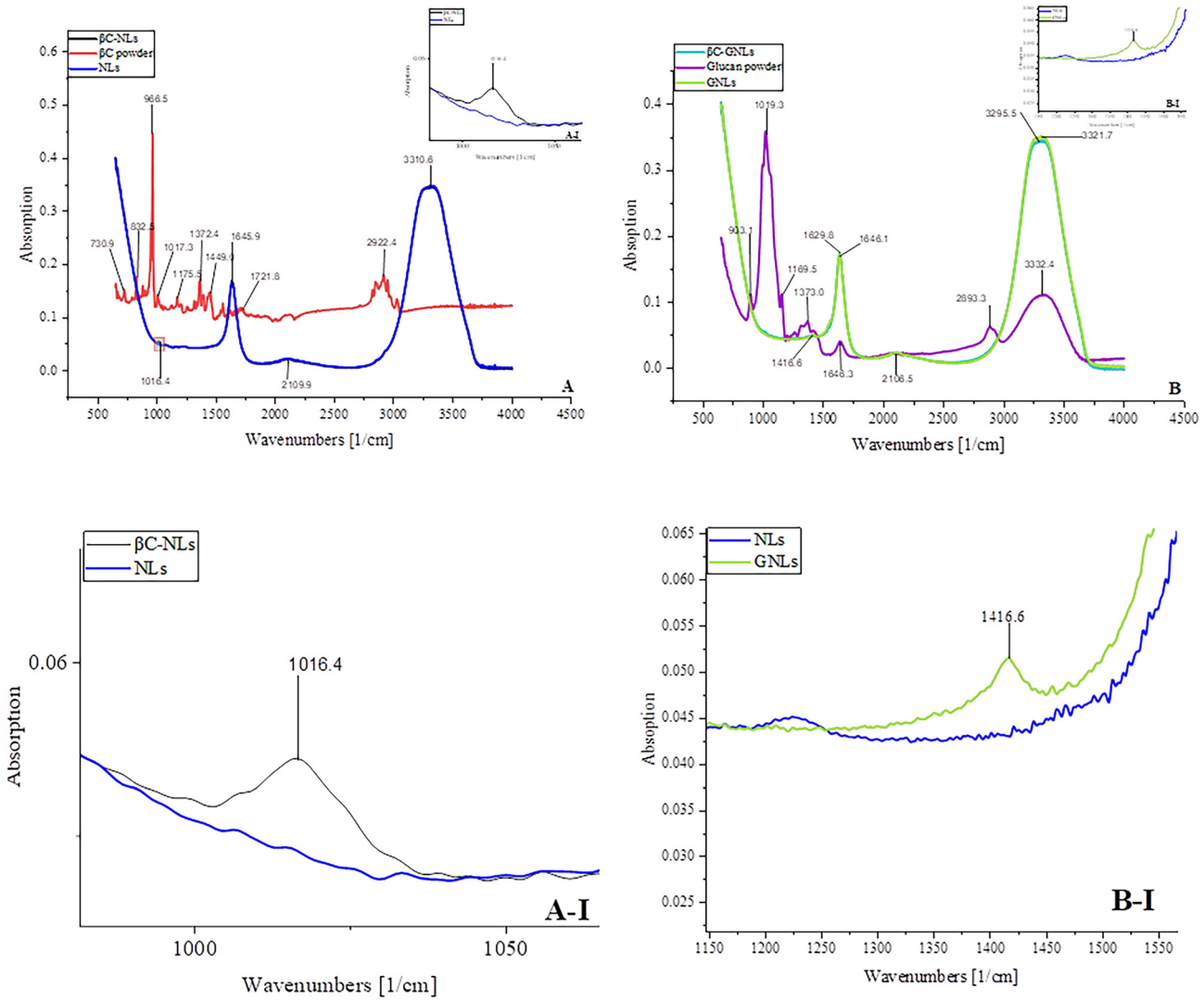

Fig. 2 Fourier transform infrared spectrum of (A) βC-loaded liposome, void liposomes and βC (powder) (B) beta-glucan powder, βC-loaded and void glucan coated liposomes (A–I) beta carotene loaded NLs and void NLs and (B–I) Difference in the FTIR spectrum of NLs and GNLs.

the major absorption band of |GNLs no noticeable change in the FTIR absorption spectrum of βC loaded GNLs was observed. That is why it can be concluded that all the encapsulated βC is present inside the core (NLs structure) and did not interact with βG layer.

3.4 Physical stability of nanosystems during *in vitro* gastrointestinal digestion

For any oral nano-delivery vesicle, stability during gastrointestinal digestion is the key factor to consider. To enhance the antioxidant activity, bioaccessibility and subsequent absorption by enterocytes of the encapsulated agent a delivery vesicle must survive the gastric environment and reach the intestinal phase intact. Therefore, we exposed βC-GNLs and βC-NLs to simulated gastrointestinal digestion. As observed previously, the phospholipid bilayer of NLs is prone to hydrolysis or disruption in a strongly acidic environment.[66] To evaluate the effect of βG coating on the stability of NLs we measured the size, charge and PDI of loaded vesicles in simulated gastrointestinal fluid (Fig. 3A & B).

Initially, the particle size and PDI of the βC-NLs and βC-GNLs were smaller, the particle size was 108 and 177 nm, and the PDI was 0.10 and 0.23, respectively. A statistically significant increase in particle size of NLs occurred during the gastric phase compared to the initial values, reaching 452 ± 20 nm in the first 60 minutes of gastric digestion (G1) and 638 ± 68 nm after 120 minutes of gastric digestion (G2). This could be related to the decrease in pH to 3 in the gastric phase, which modified the strength and range of colloidal interaction between NLs, allowing coalescence to occur, thereby increasing their size.[67] Similarly, higher PDI values of NLs during the gastric phase 0.62 PDI for G1 and 0.72 PDI for G2 indicate the heterogeneity in size distribution during this phase. Continuous decrease in ZP values of NLs from the initial to end phase (Fig. 3B) of simulated digestion also represents low stability of NLs. A significant decrease in the size of βC-NLs

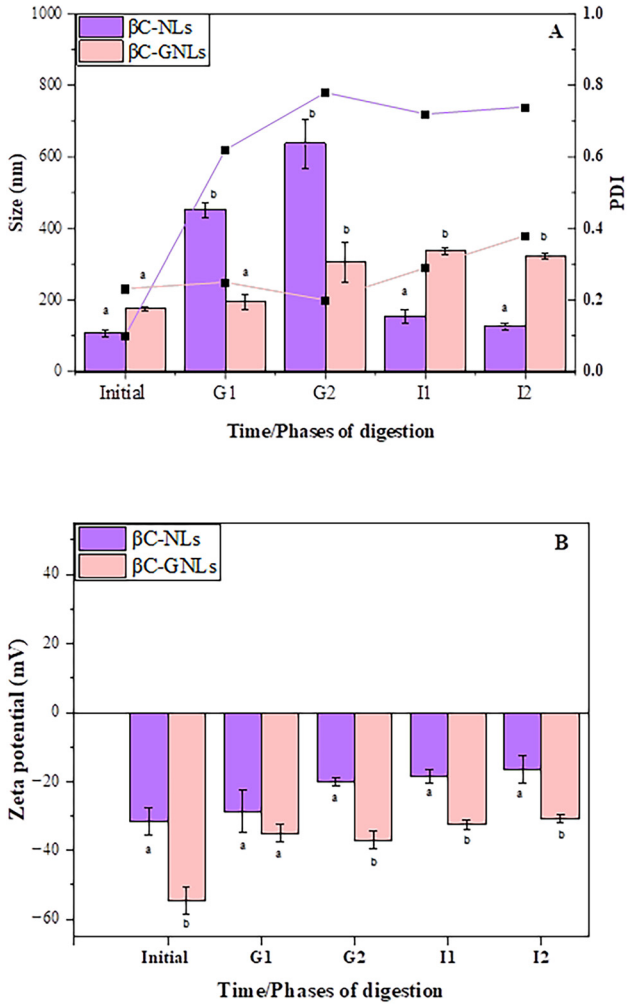

Fig. 3 Physical stability of βC-NLs and βC-GNLs during simulated gastrointestinal digestion at different times (n = 3). (A) Size stability and PDI; (B) zeta potential. Purple and pink bars represents the size of βC-NLs and βC-GNLs respectively, while different color line in the graph represents the PDI. Values are the means ± SD (n = 6). Different letters represent a significant difference ($p < 0.05$).

(I1: 155 ± 40 nm, I2 127 ± 11 nm) was observed in the intestinal phase of digestion. This size decrease could be due to the emulsification effect of bile salts on NLs as well as the hydrolysis of the phospholipids by intestinal enzymes, which would decrease particle size. Additionally, the size reduction of NLs at this stage may also be due to the release of the entire encapsulated agent and taken up by the mixed micelles. The higher PDI value of uncoated NLs confirmed that the intestinal fluid contained mixed micelles and mixed bilayers after 120 min of intestinal digestion. Comparable results were observed previously where β-carotene-loaded liposomes demonstrated remarkable changes in size and PDI during digestion in the intestinal phase.[68]

In contrast, βC-GNLs demonstrated only a slight increase in size (195 ± 21 after 60 min of gastric digestion and 308 ± 55 nm after 120 minutes of gastric digestion) during gastric digestion (Fig. 3A). However, size remained homogeneous (PDI ≥ 0.3) throughout the gastrointestinal digestion. Furthermore, the ZP remaining above −30 mV also confirms the higher stability of GNLs. From these results, we could suggest that βG coating not only protected liposomes against acid degradation but also prevented leakage of encapsulated beta-carotene during gastrointestinal digestion.

3.5 Controlled release and bioaccessibility

To understand the effect of pH & gastric and intestinal enzymes on the controlled release and eventually on the bioaccessibility of βC from uncoated (NLs) beta glucan-coated NLs (βC-GNLs), nano-encapsulated βC was subjected to static *in vitro* gastrointestinal digestion. As presented in Fig. 4A overall the release rate of βC from NLs was higher than the βC encapsulated in GNLs. Almost 26% of βC was released from NLs after two hours of gastric digestion, which raised to 56% after 2 h of intestinal digestion. The slow-release rate of βC during gastric digestion could be attributed to the lack of gastric lipase in the digestion model.[69] On the other hand, the massive release of βC from NLs during intestinal digestion was due to the interaction of pancreatic enzymes and bile salts with the lipid bilayer structure. Lipid hydrolysis produced mixed micelles to dissolve encapsulated nutrients, which results in higher βC release. After 4 h of *in vitro* digestion, the cumulative release of βC from GNLs was only 10% and 15%, in the gastric and intestinal phases, respectively.

Our results suggest that βG coating protects liposome-containing βC from hydrolysis by intestinal enzymes and a much lower amount of βC was released even after 2 hours of intestinal digestion. It was observed previously that polymer coatings on NLs act as a barrier, do not allow digestive enzymes and bile salts to reach the liposomal structure and maintain the integrity of the core nanostructure.[70,71] Therefore, we can say that strong steric hindrance effect provided by the βG coating play a significant role in the stability of GNLs during *in vitro* simulated digestion, which decreases the access of digestive enzymes to the lipid, protect encapsulated agent and core NLs from being hydrolysed hence, provide slow release of the encapsulated agent.

These results are in accordance with the bioaccessibility data where we could see the higher amount of bio-accessible βC after βC-NL digestion (88.3 ± 9%) while only 38 ± 11% bioaccessibility of βC was observed after βC-GNLs digestion (Fig. 1B). This means almost all the encapsulated βC in uncoated NLs is released and available in the mixed micelles phase. This high bioaccessibility attributed to the higher extent of lipolysis by the pancreatin enzyme results in more lipid digestion products being in the mixed micelles, which contributes to the larger bioaccessibility of hydrophobic nutraceuticals. Similar results were observed previously by Yi (2015), he observed better bioaccessibility of β-carotene with the growing concentration of pancreatin and lipase during digestion.[72]

In GNLs, glucan coating steric hindrance protect the core NLs structure from being hydrolyse, prevented release of encapsulated βC from the core NLs and only a limited amount

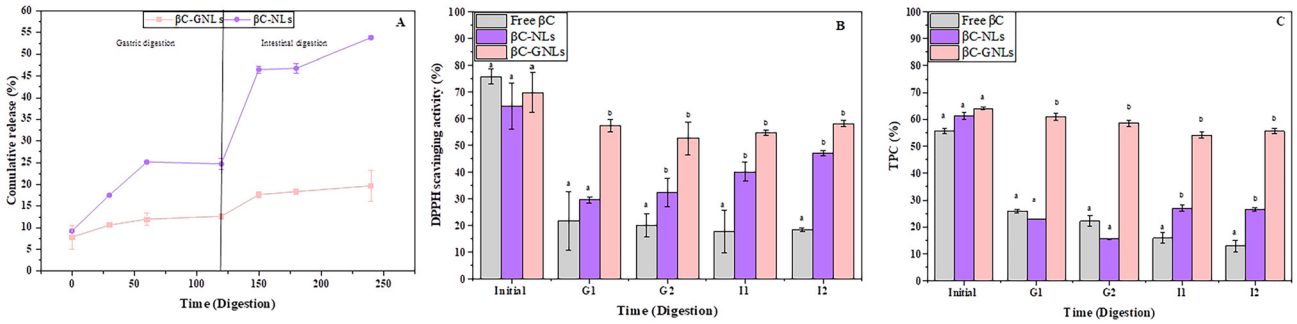

Fig. 4 (A) *In vitro* controlled release βC from βC-NLs and βC-GNLs, (B) DPPH (C) total phenolic content represents free and nano-encapsulated βC during gastrointestinal digestion. Data are mean (n = 3) ±standard deviation (SD). Columns with different letters represents significant difference from each other at $p < 0.05$.

of βC was available for mixed micelles, therefore, it was less bioaccessible. Another reason behind the low bioaccessibility of the βC encapsulated in GNLs could be their negative charges, which could inhibit the attachment of anionic bile salts and free-fatty acids to the surface of glucan-modified NLs[73] resulting in less mixed micelles formation and low bioaccessibility of the encapsulated agent. Furthermore, due to high viscosity of the βG polymer it could entrap mixed micelles that would also reduce the bioaccessibility of βC. Previously, it was observed that DF can inhibit micelle formation and decrease β-carotene (βC) bioavailability *in vitro* and *in vivo*.[74] As βG is a high viscosity DF and is resistant to gastrointestinal digestion, it can inhibit micelle formation and reduce β-carotene bioaccessibility *in vitro*.

3.6 Antioxidant activity of βC-loaded glucan modified NLs

The antioxidative activities of free βC and βC-loaded nanocarriers were evaluated by the DPPH method during the simulated gastrointestinal environment (37 °C). Free/unencapsulated βC is more prone to isomerization and degradation during *in vitro* digestion, which led to a notable change in its antioxidant capacity. We observed continuous reduction in the antioxidant activity of free beta-carotene during gastrointestinal digestion when compared with undigested βC (75.8 ± 2.8%). On the other hand, βC-NLs displayed higher radical scavenging activity than free βC (Fig. 4B). However, activity was much less during gastric as well as in intestinal digestion than in the initial undigested samples (64.8 ± 8.6%). DPPH scavenging activity of βC-NLs initially decreased and then increased with the increase of digestion time. It was 29.5 ± 1.2% in the first 60 minutes and then increased to 32.4 ± 1.3%, 40.1 ± 3.5% and 47.1 ± 1.04% after 120, 180, and 240 minutes of digestion, respectively. This low DPPH scavenging activity during the gastric phase could be due to the coalescence or aggregation of NLs during gastric digestion. Before digestion antioxidant, activity of the βC-GNLs was 69.8 ± 7.4, which remains consistent during digestion, and 58.2 ± 1% antioxidant activity can be observed at the end of the GI digestion (Fig. 4B). Overall, the scavenging ability of glucan-coated NLs to DPPH radicals was higher than uncoated NLs.

Similar results were observed with TPC of the samples (Fig. 4C), where GNLs had a higher level of phenolic content before and after *in vitro* digestion than uncoated NLs. These results can be explained by several factors. First, βG coating had a better protective effect on core components and prevented its degradation by digestive enzymes. Secondly, synergistic antioxidant (AO) activity of βG, core layer and encapsulated agent (beta-carotene) would result in higher AO activity. Additionally, glycosidic bonds in high molecular weight βG break during size reduction to nanoscale leading to the exposure of hydroxyl groups in β-glucan and decrease the intramolecular hydrogen bonding that increased the radical scavenging activity and TPC of GNLs.

3.7 Multiple particle tracking

It has been reported previously that DF like β-glucan (βG) can reduce the permeability of intestinal mucus by altering the microviscosity of the mucus.[75] That is why it was important to investigate the effect of beta glucan-coated nanocarriers on microviscosity and subsequent diffusion as well as absorption by intestinal mucus. For this purpose, we performed multiple particle tracking using a high-resolution confocal microscope to track the individual trajectories of 50–120 fluorescently labelled nanocarriers. The mean square displacement (MSD) was calculated at one second intervals and from mean ⟨MSD⟩ values diffusion coefficients (D_{eff}), exponential anomaly (α), and microviscosity was calculated (Fig. 5).

The ⟨MSD⟩ of GNLs was significantly lower than the uncoated NLs. Diffusivity of the GNLs was slightly more restricted by mucus than the uncoated NLs (Fig. 5B). That could be due to the mucoadhesive nature of glucan, more negative charge, and bigger size of GNLs than NLs. Particle diffusion in mucus is often restricted and described as 'sub-diffusive' with exponential anomalous (α) value < 1. Alpha values between 0.2 and 0.9 reflect varying degrees of interference to particle movement. The alpha value of GNLs and NLs were 0.80 ± 0.01 and 0.91 ± 0.001 respectively (Fig. 5C), which suggest that GNLs had more interaction with mucus than NLs and both particles demonstrate sub-diffusion in pig intestinal mucus. An alpha value of less than 0.2 represents

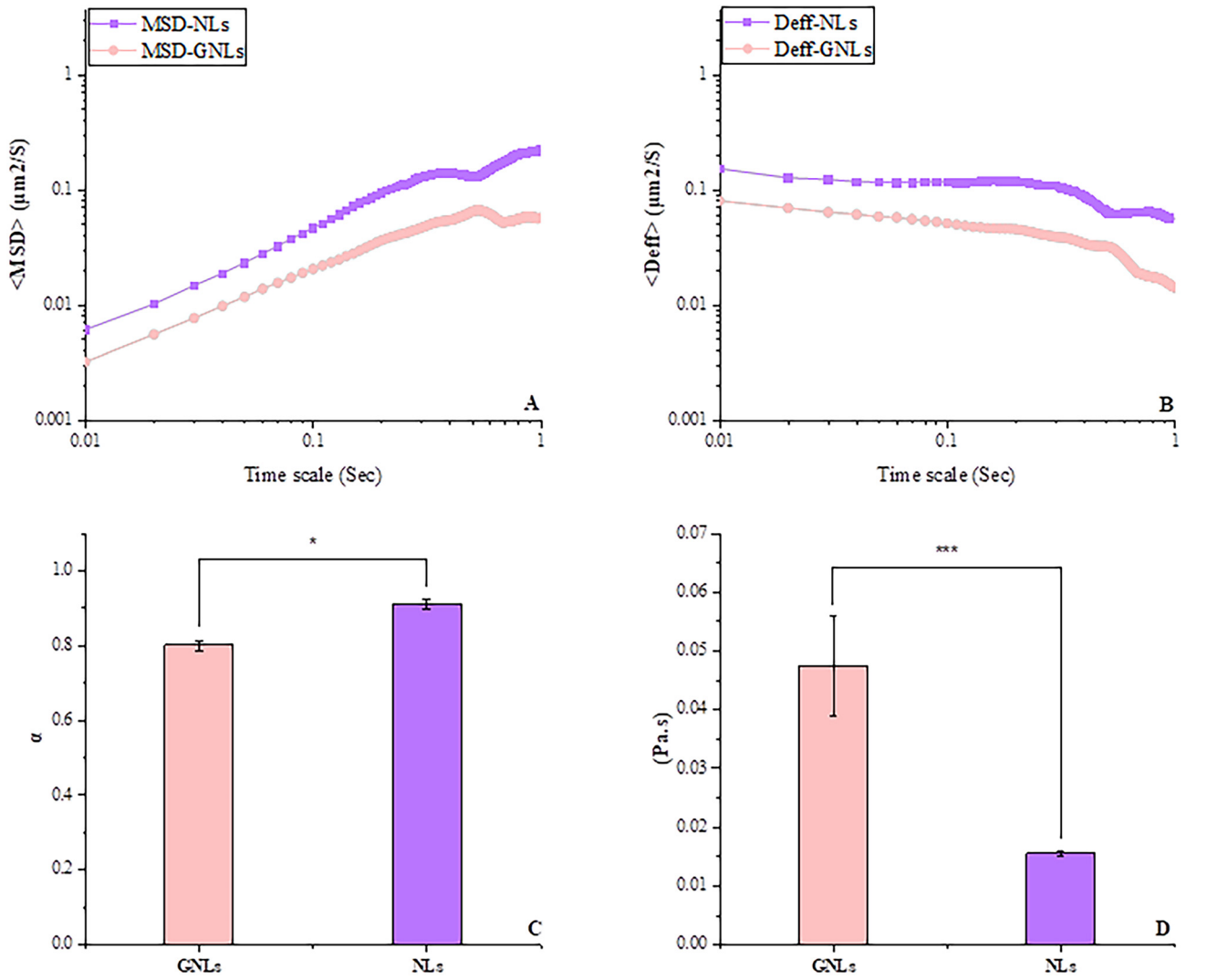

Fig. 5 Multiple particle tracking (MPT) results of fluorescently labelled NLs and GNLs in pig intestinal mucus (A) MSD as a function of time, $n = 3$; (B) diffusion coefficients (D_{eff}), (C) exponential anomalous (α) and (D) microviscosity. The number of particles analysed in each test were >50. Values are the means $n = 3 \pm$ SD (***$P < 0.05$, *$P < 0.01$).

complete immobilization with no diffusion and stronger interaction between mucus and particle.[76]

As previously claimed in many studies that the particle diffusion in mucus and their subsequent absorption by intestinal cells can be effected by many factors *i.e.*, shape, size, charge, hydrophobicity and surface chemistry of the particle as well as pH of the medium.[5,77–79]

Size of the GNLs was observed to be 300 nm after two hours of intestinal digestion, however size of the uncoated liposomes was around 100 nm (Fig. 3A). Previously it was observed that the particles with a smaller size than the mucus microstructure can effectively diffuse through the mucus without any hindrance and the diffusion through mucus decreases with increasing particle size.[80,81] These studies suggest that the particles with size ranges from 50–100 nm have greater potential to permeate across the mucus layer than ≥200 nm particles.[66] Similarly, another study suggests that coating by dense biopolymers nanoparticle size below the mucus meshwork size can diffuse through the mucus and achieve a higher absorption of encapsulated agent, but this diffusion would be slightly restricted than the uncoated nanoparticles.[82]

Other important that could effect the particle diffusion in mucus is their surface charge. Overall mucus contain net negative charge therefore Positively charged nanoparticles would show more strong electrostatic interaction with mucus, there proves to be less mucopenetrating and more mucoadhesive. Small negatively charged particles like NLs are more slippery owing to the repulsive forces. Hence can diffuse faster than the cationic particles.[83] Although the charge on the GNLs was also negative but we observe less diffusion of GNLs than liposomes so we could suggest that in a bigger size particle electrostatic repulsion from the similarly charged entity (mucus) would provide more hindrance and make it more difficult to diffuse freely in the mucus. Furthermore, other factors like

high mucoadhesive and low lipophilic nature of beta glucan would also reduce the diffusion of GNLs than phospholipids based NLs.

It was stated previously that the β-glucan can directly interact with the gastrointestinal mucosa and then transferred to the blood circulation, it can also affect the microviscosity of the mucus.[84] We also observe the difference in microviscosity of the porcine intestinal mucus after interaction with coated and uncoated NLs (Fig. 5D). Higher microviscosity of mucus with GNLs proves that GNLs interaction with mucus is higher than the uncoated NLs. Which can be attributed to the bigger size GNLs and viscous nature of βG, due to which GNLs interact more with mucus polymeric mesh. While on the other hand NLs can directly diffuse through the mucus layer without any interaction or hurdle. Multiple particle tracking data suggest that βG coated NLs face more hindrance during diffusion through the mucus than uncoated NLs. Which would increase the residence time of GNLs in the mucus and affect the absorption of nanocarriers and encapsulated active agent.

3.8 *Ex vivo* transports of dietary fiber-coated nanocarriers *via* intestinal mucosa of rats in Ussing chambers

After digestion, controlled release and bioaccessibility data suggest that GNLs were unable to hydrolyse by digested enzymes and small amount of βC was available in micellar form to get absorbed by intestinal epithelial cells. Conversely, hydrolysis of uncoated NLs by pancreatin lipase and bile salt makes βC encapsulated in NLs more bioaccessible. GNLs remain intact after digestion with all the βC still encapsulated inside so the question arises will these nanocarriers be able to transport/absorb directly *via* the intestinal epithelium layer to make encapsulated βC more bioavailable or not? To answer this question, we perform an Ussing chamber experiment with mouse intestinal tissue and measured the amount of βC on the basolateral and apical side of the tissue.

According to the literature, nanoparticle absorption occurs mostly in the jejunum and ileum through non-specific endocytosis similarly βC absorption also occurs in the duodenum and jejunum.[17] Therefore, considering the absorption sites of both β-carotene and nanoparticles, we selected the jejunum of the mouse intestine in the Ussing chamber experiment. Digested samples of βC-NLs and βC-GNLs were added to the apical side of the tissue mounted in the Ussing chamber, samples were extracted at a specific time intervals from the basolateral as well as from the apical side and the concentration of βC was calculated. The amount of βC present in tissue was also extracted and quantified at the end of the experiment (after 130 min). It was observed that the permeation/absorption of βC from both (coated and uncoated) nanocarriers increase over time. However, the absorption of beta-carotene encapsulated in GNLs was lower than the βC-NLs. The amount of βC available on the basolateral side from βC-NLs digest was 50.48 ± 2.5 and 61.54 ± 3 ng mL^{-1} after 80 and 130 minutes respectively (Fig. 6). At the same time intervals only 20 ± 1 and 27.7 ± 1.3 ng mL^{-1} of βC was,

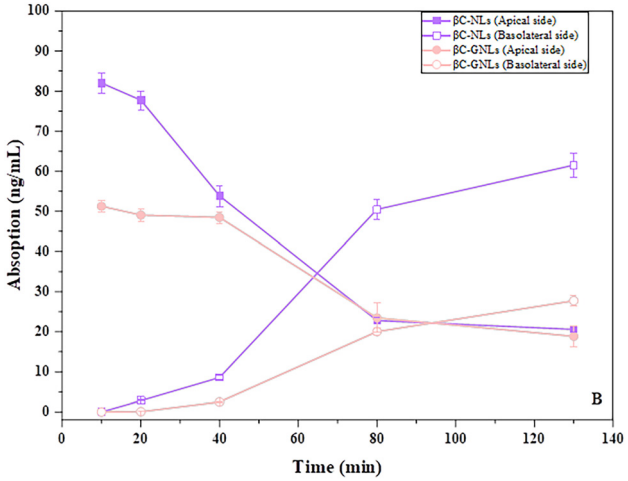

Fig. 6 Absorption of βC-NLs and βC-GNLs across rat jejunum in Ussing chambers. Open circle and square represent the amount of βC present on the basolateral side; closed circle and square represent the amount of βC on the apical side of the rat jejunal tissue. The purple color line in the graph represents βC-NLs while pink represents the βC-GNLs. Data are presented as mean (n = 2) ±SD and the absorption of βC-NLs (basolateral side) and βC-GNLs (basolateral side) are significantly different from each other at 40, 80 and 130minutes ($p < 0.05$).

absorbed through the intestinal cells from digested βC-GNLs. This lower absorption could also be related to the low bioaccessibility of βC loaded in DF-coated NLs than uncoated NLs. That could be related to the fact the liposomes were readily accessed by lipase and promote the formation of mixed micelles, thus enhancing the uptake of β-carotene. While on the other hand, due to beta glucan coating GNLs were not accessible for digestion enzymes that reduce mixed micelles formation, hence reduce the absorption of βC. Secondly, mucoadhesive and viscous properties of beta-glucan[85] can increase the intestinal resident time of βC-GNLs, reduce the diffusion of GNLs into the mucus hence decrease its permeability than the uncoated NLs.

By the end of the experiment, 12.5 ng βC was extracted from the tissue treated with GNLs while only 2.58 ng βC was extracted from the tissue treated with NLs. From these results, we can conclude that βC-GNLs could be trapped in the epithelial mucus layer that would reduce the absorption and increase the residence time of GNLs in the mucus. This slow rate of epithelial absorption of βC-GNLs might prolong the bioavailability of the encapsulated agent. While on the other hand, uncoated NLs penetrate through the epithelial mucus more rapidly without any hindrance resulted in higher absorption rate of βC encapsulated in NLs. These results matches the previous studies were it was observed that the particle size and composition of the nanocarrier systems could greatly affect the absorption of encapsulated beta-carotene. Nano carriers with particle size below than 200 nm and having lipid based composition can diffuse more through mucosal lining and can get absorbed more quickly by the enterocyte, than bigger size particles having other macromolecular based composition.[86]

4. Conclusion and perspectives

In this study, beta glucan-coated nanoliposomes (GNLs) were prepared to investigate the effect of DF coating on the stability, controlled release, antioxidant activity, and bioaccessibility of βC during gastrointestinal digestion. Diffusion of GNLs through pig intestinal mucus and their absorption through the intestinal epithelial layer were also investigated. GNLs demonstrated high encapsulation efficiency, and physical stability, remained intact during first-pass metabolism and provided sustained release of β during GI digestion. Our data suggest that the βG coating protects core liposomes and encapsulated agents from digestive enzyme hydrolysis, which results in low mixed micelle production and eventually low bioaccessibility of the encapsulated βC in GNLs. Similarly, MPT analysis confirms that due to higher interaction between GNLs and mucus polymeric mesh, diffusion rate of GNLs in mucus was lower than the uncoated NLs. This low diffusion effects their permeability through the mucusepithelial layer. Therefore, Uptake/absorption of βC encapsulated in GNLs by rat jejunum cells was also significantly lower than the βC-NLs.

Unlike many previous studies where bioaccessibility and bioavailability of lipophilic nano-encapsulated compounds improve after βG-based bio-polymeric coatings, our data suggest that βG coating does not allow the release of βC during intestinal phase due to which bioaccessibility of active compounds was reduced. Additionally, slow diffusion rate of GNLs through intestinal mucus reduces the absorption of βC through intestinal epithelium than the uncoated NLs. From our investigation, we can suggest that βG-coated nanoliposomes act as a potential NCS to provide sustained release, longer retention time in mucus and slow absorption of active agents to attain prolonged bioavailability. GNLs might provide beneficial effects where colon-specific delivery of active agents is required. Gut microbiota can play a significant role to digest the glucan coating hence, the higher bioaccessibility of active agents could be observe in the colon.

In perspective, further investigation with other DF-based nanoparticles (especially water-soluble dietary fibre) is required to understand their effect on mucus permeability, absorption, and uptake *via* the intestinal lumen after digestion. Evaluation of bioaccessibility and uptake of GNLs by colon cells. Different concentrations of dietary fibre should be tested to evaluate the concentration-dependent effect of these biopolymers on the bioaccessibility and bioavailability of nano-encapsulated active agents.

Author contributions

Taskeen Niaz: conceptualization, methodology, investigation, writing – original draft. Alan Mackie: conceptualization, writing – review & editing, supervision, project administration.

Conflicts of interest

The authors declare that there is no conflict of interest regarding the publication of this article.

Acknowledgements

The authors gratefully acknowledge the School of Food Science and Nutrition (University of Leeds, UK) for providing all the technical and financial support in this work.

References

1 S. Manocha, S. Dhiman, A. S. Grewal and K. Guarve, Nanotechnology: An approach to overcome bioavailability challenges of nutraceuticals, *J. Drug Delivery Sci. Technol.*, 2022, **72**, 103418.
2 N. A. Helal, H. A. Eassa, A. M. Amer, M. A. Eltokhy, I. Edafiogho and M. I. Nounou, Nutraceuticals' novel formulations: the good, the bad, the unknown and patents involved, *Recent Pat. Drug Delivery Formulation*, 2019, **13**, 105–156.
3 T. Niaz, S. Shabbir, T. Noor and M. Imran, Antimicrobial and antibiofilm potential of bacteriocin loaded nano-vesicles functionalized with rhamnolipids against foodborne pathogens, *LWT*, 2019, **116**, 108583.
4 Z. Azarashkan, S. Farahani, A. Abedinia, M. Akbarmivehie, A. Motamedzadegan, J. Heidarbeigi and A. A. Hayaloğlu, Co-encapsulation of broccoli sprout extract nanoliposomes into basil seed gum: effects on in vitro antioxidant, antibacterial and anti-Listeria activities in ricotta cheese, *Int. J. Food Microbiol.*, 2022, 109761.
5 A. H. Hamadou, W.-C. Huang, C. Xue and X. Mao, Comparison of β-carotene loaded marine and egg phospholipids nanoliposomes, *J. Food Eng.*, 2020, **283**, 110055.
6 T. Ghorbanzade, S. M. Jafari, S. Akhavan and R. Hadavi, Nano-encapsulation of fish oil in nano-liposomes and its application in fortification of yogurt, *Food Chem.*, 2017, **216**, 146–152.
7 H. Cui, C. Zhao and L. Lin, The specific antibacterial activity of liposome-encapsulated Clove oil and its application in tofu, *Food Control*, 2015, **56**, 128–134.
8 C. Sebaaly and H. Greige-Gerges, in *Liposomal Encapsulation in Food Science and Technology*, ed. C. Anandharamakrishnan and S. Dutta, Academic Press, 2023, pp. 125–144, DOI: 10.1016/B978-0-12-823935-3.00008-4.
9 T. Niaz, S. Shabbir, T. Noor and M. Imran, Active Composite Packaging Reinforced with Nisin-Loaded Nano-Vesicles for Extended Shelf Life of Chicken Breast Filets and Cheese Slices, *Food Bioprocess Technol.*, 2022, 1–15.
10 M. Marsanasco and S. d. V. Alonso, Physicochemical, functional, and sensory characterization of orange juice containing food additives with bioactive compounds under

heat treatment and storage conditions, *Food Biosci.*, 2021, **44**, 101393.

11 C. Hernandez and S. Shukla, Liposome based drug delivery as a potential treatment option for Alzheimer's disease, *Neural Regener. Res.*, 2022, **17**, 1190.

12 S. Cantor, L. Vargas, A. O. E. Rojas, C. J. Yarce, C. H. Salamanca and J. Oñate-Garzón, Evaluation of the antimicrobial activity of cationic peptides loaded in surface-modified nanoliposomes against foodborne bacteria, *Int. J. Mol. Sci.*, 2019, **20**, 680.

13 S. F. Hosseini, M. Soofi and M. Rezaei, Enhanced physicochemical stability of ω-3 PUFAs concentrates-loaded nanoliposomes decorated by chitosan/gelatin blend coatings, *Food Chem.*, 2021, **345**, 128865.

14 S. Liu, J. Lian, Z. Xu, Y. Ning, M. Shi, Z. Zhao and Z. Zhang, Chitosan-coated nanoliposomes for efficient delivery of betanin with enhanced stability and bioavailability, *Food Hydrocolloids*, 2022, **132**, 107871.

15 T. Niaz, S. Shabbir, T. Noor, A. Rahman, H. Bokhari and M. Imran, Potential of polymer stabilized nano-liposomes to enhance antimicrobial activity of nisin Z against foodborne pathogens, *LWT*, 2018, **96**, 98–110.

16 S. Amjadi, H. Almasi, H. Hamishehkar, M. A. Khaledabad and L.-T. Lim, Coating of betanin and carvone Co-loaded nanoliposomes with synthesized cationic inulin: A strategy for enhancing the stability and bioavailability, *Food Chem.*, 2022, **373**, 131403.

17 G. Liu, Y. Zhou and L. Chen, Intestinal uptake of barley protein-based nanoparticles for β-carotene delivery, *Acta Pharm. Sin. B*, 2019, **9**, 87–96.

18 Y. Cao, X. Dong and X. Chen, Polymer-modified liposomes for drug delivery: from fundamentals to applications, *Pharmaceutics*, 2022, **14**, 778.

19 N. Efsa, Panel on Dietetic Products and Allergies, Scientific Opinion on the substantiation of health claims related to beta–glucans from oats and barley and maintenance of normal blood LDL–cholesterol concentrations (ID 1236, 1299), increase in satiety leading to a reduction in energy intake (ID 851, 852), reduction of post–prandial glycaemic responses (ID 821, 824), and "digestive function"(ID 850) pursuant to Article 13 (1) of Regulation (EC) No 1924/2006, *EFSA J.*, 2011, **9**, 2207.

20 J. Yu, J. Xia, C. Yang, D. Pan, D. Xu, G. Sun and H. Xia, Effects of oat beta-glucan intake on lipid profiles in hypercholesterolemic adults: A systematic review and meta-analysis of randomized controlled trials, *Nutrients*, 2022, **14**, 2043.

21 E. Llanaj, G. M. Dejanovic, E. Valido, A. Bano, M. Gamba, L. Kastrati, B. Minder, S. Stojic, T. Voortman and P. Marques-Vidal, Effect of oat supplementation interventions on cardiovascular disease risk markers: a systematic review and meta-analysis of randomized controlled trials, *Eur. J. Nutr.*, 2022, 1–30.

22 A. F. Cicero, F. Fogacci, M. Veronesi, E. Strocchi, E. Grandi, E. Rizzoli, A. Poli, F. Marangoni and C. Borghi, A randomized placebo-controlled clinical trial to evaluate the medium-term effects of oat fibers on human health: the beta-glucan effects on lipid profile, glycemia and intestinal health (BELT) study, *Nutrients*, 2020, **12**, 686.

23 S. A. Joyce, A. Kamil, L. Fleige and C. G. Gahan, The cholesterol-lowering effect of oats and oat beta glucan: modes of action and potential role of bile acids and the microbiome, *Front. Nutr.*, 2019, **6**, 171.

24 V. H. Telle-Hansen, L. Gaundal, B. Høgvard, S. M. Ulven, K. B. Holven, M. G. Byfuglien, I. Måge, S. H. Knutsen, S. Ballance and A. Rieder, A three-day intervention with granola containing cereal beta-glucan improves glycemic response and changes the gut microbiota in healthy individuals: A crossover study, *Front. Nutr.*, 2022, **9**, 796362.

25 C. Villemejane, S. Denis, A. Marsset-Baglieri, M. Alric, P. Aymard and C. Michon, In vitro digestion of short-dough biscuits enriched in proteins and/or fibres using a multi-compartmental and dynamic system (2): Protein and starch hydrolyses, *Food Chem.*, 2016, **190**, 164–172.

26 A. R. Mackie, A. Macierzanka, K. Aarak, N. M. Rigby, R. Parker, G. A. Channell, S. E. Harding and B. H. Bajka, Sodium alginate decreases the permeability of intestinal mucus, *Food Hydrocolloids*, 2016, **52**, 749–755.

27 N. Mäkelä, N. Rosa-Sibakov, Y.-J. Wang, O. Mattila, E. Nordlund and T. Sontag-Strohm, Role of β-glucan content, molecular weight and phytate in the bile acid binding of oat β-glucan, *Food Chem.*, 2021, **358**, 129917.

28 A. Shah, Z. ul Ashraf, A. Gani, F. A. Masoodi and A. Gani, β-Glucan from mushrooms and dates as a wall material for targeted delivery of model bioactive compound: Nutraceutical profiling and bioavailability, *Ultrason. Sonochem.*, 2022, **82**, 105884.

29 X. Xiao, C. Tan, X. Sun, Y. Zhao, J. Zhang, Y. Zhu, J. Bai, Y. Dong and X. Zhou, Effects of fermentation on structural characteristics and in vitro physiological activities of barley β-glucan, *Carbohydr. Polym.*, 2020, **231**, 115685.

30 J. Hwang, K. Lee, A. A. Gilad and J. Choi, Synthesis of beta-glucan nanoparticles for the delivery of single strand DNA, *Biotechnol. Bioprocess Eng.*, 2018, **23**, 144–149.

31 R. Parthasarathy, S. P. Kumar, H. C. Y. Rao and J. Chelliah, Synthesis of β-Glucan Nanoparticles from Red Algae–Derived β-Glucan for Potential Biomedical Applications, *Appl. Biochem. Biotechnol.*, 2021, **193**, 3983–3995.

32 A. S. Cordeiro, Y. Farsakoglu, J. Crecente-Campo, M. de la Fuente, S. F. González and M. J. Alonso, Carboxymethyl-β-glucan/chitosan nanoparticles: new thermostable and efficient carriers for antigen delivery, *Drug Delivery Transl. Res.*, 2021, **11**, 1689–1702.

33 A. E. Kaziem, L. Yang, Y. Lin, A. E. Kazem, H. Xu and Z.-x. Zhang, Pathogenic Invasion-Responsive Carrier Based on Mesoporous Silica/β-Glucan Nanoparticles for Smart Delivery of Fungicides, *ACS Sustainable Chem. Eng.*, 2021, **9**, 9126–9138.

34 V. K. Maurya, A. Shakya, M. Aggarwal, K. M. Gothandam, T. Bohn and S. Pareek, Fate of β-carotene within loaded delivery systems in food: state of knowledge, *Antioxidants*, 2021, **10**, 426.

35 V. Komalla, V. S. R. R. Allam, P. C. L. Kwok, B. Sheikholeslami, L. Owen, A. Jaffe, S. A. Waters, S. Mohammad, B. G. Oliver and H. Chen, A phospholipid-based formulation for the treatment of airway inflammation in chronic respiratory diseases, *Eur. J. Pharm. Biopharm.*, 2020, **157**, 47–58.
36 T. Niaz, A. Sarkar, A. Mackie and M. Imran, Impact of albumin corona on mucoadhesion and antimicrobial activity of carvacrol loaded chitosan nano-delivery systems under simulated gastro-intestinal conditions, *Int. J. Biol. Macromol.*, 2021, **169**, 171–182.
37 C. Bai, J. Zheng, L. Zhao, L. Chen, H. Xiong and D. J. McClements, Development of oral delivery systems with enhanced antioxidant and anticancer activity: coix seed oil and β-carotene coloaded liposomes, *J. Agric. Food Chem.*, 2018, **67**, 406–414.
38 Y. Shi, F. Ye, Y. Zhu and M. Miao, Development of dendrimer-like glucan-stabilized Pickering emulsions incorporated with β-carotene, *Food Chem.*, 2022, **385**, 132626.
39 X. Liu, P. Wang, Y.-X. Zou, Z.-G. Luo and T. M. Tamer, Co-encapsulation of Vitamin C and β-Carotene in liposomes: Storage stability, antioxidant activity, and in vitro gastrointestinal digestion, *Food Res. Int.*, 2020, **136**, 109587.
40 T. Niaz, S. Shabbir, T. Noor, R. Abbasi, Z. A. Raza and M. Imran, Polyelectrolyte multicomponent colloidosomes loaded with nisin Z for enhanced antimicrobial activity against foodborne resistant pathogens, *Front. Microbiol.*, 2018, **8**, 2700.
41 T. Niaz, M. Imran and A. Mackie, Improving carvacrol bioaccessibility using core–shell carrier-systems under simulated gastrointestinal digestion, *Food Chem.*, 2021, **353**, 129505.
42 A. Brodkorb, L. Egger, M. Alminger, P. Alvito, R. Assunção, S. Ballance, T. Bohn, C. Bourlieu-Lacanal, R. Boutrou and F. Carrière, INFOGEST static in vitro simulation of gastrointestinal food digestion, *Nat. Protoc.*, 2019, **14**, 991–1014.
43 C. Bai, J. Zheng, L. Zhao, L. Chen, H. Xiong and D. J. McClements, Development of Oral Delivery Systems with Enhanced Antioxidant and Anticancer Activity: Coix Seed Oil and β-Carotene Coloaded Liposomes, *J. Agric. Food Chem.*, 2019, **67**, 406–414.
44 J. Rumpf, R. Burger and M. Schulze, Statistical evaluation of DPPH, ABTS, FRAP, and Folin-Ciocalteu assays to assess the antioxidant capacity of lignins, *Int. J. Biol. Macromol.*, 2023, **233**, 123470.
45 M. Le Berre, J. Q. Gerlach, M. E. Gallagher, L. Joshi, S. D. Carrington and M. Kilcoyne, Mucin Purification and Printing Natural Mucin Microarrays, *Glycan Microarrays: Methods and Protocols*, Springer Nature, 2022, pp. 127–146.
46 Y. Wu, W. Wang, Z. Yu, K. Yang, Z. Huang, Z. Chen, X. Yan, H. Hu and Z. Wang, Mushroom-brush transitional conformation of mucus-inert PEG coating improves co-delivery of oral liposome for intestinal metaplasia therapy, *Biomater. Adv.*, 2022, 212798.
47 A. Macierzanka, A. R. Mackie and L. Krupa, Permeability of the small intestinal mucus for physiologically relevant studies: Impact of mucus location and ex vivo treatment, *Sci. Rep.*, 2019, **9**, 1–12.
48 A. Macierzanka, A. R. Mackie and L. Krupa, Permeability of the small intestinal mucus for physiologically relevant studies: Impact of mucus location and ex vivo treatment, *Sci. Rep.*, 2019, **9**, 17516.
49 C. Guan, Y. Yang, D. Tian, Z. Jiang, H. Zhang, Y. Li, J. Yan, C. Zhang, C. Chen and J. Zhang, Evaluation of an Ussing Chamber System Equipped with Rat Intestinal Tissues to Predict Intestinal Absorption and Metabolism in Humans, *Eur. J. Drug Metab. Pharmacokinet.*, 2022, **47**, 639–652.
50 A. A. Jovanović, B. D. Balanč, V. B. Djordjević, A. Ota, M. Skrt, K. P. Šavikin, B. M. Bugarski, V. A. Nedović and N. P. Ulrih, Effect of gentisic acid on the structural-functional properties of liposomes incorporating β-sitosterol, *Colloids Surf., B*, 2019, **183**, 110422.
51 K. Cacua, F. Ordoñez, C. Zapata, B. Herrera, E. Pabón and R. Buitrago-Sierra, Surfactant concentration and pH effects on the zeta potential values of alumina nanofluids to inspect stability, *Colloids Surf., A*, 2019, **583**, 123960.
52 Z. An, Z. Liu, H. Mo, L. Hu, H. Li, D. Xu and B. Chitrakar, Preparation of Pickering emulsion gel stabilized by tea residue protein/xanthan gum particles and its application in 3D printing, *J. Food Eng.*, 2023, **343**, 111378.
53 D. Hudiyanti, V. Putri, Y. Hikmahwati, S. Christa, P. Siahaan and D. Anugrah, Interaction of Phospholipid, Cholesterol, Beta-Carotene, and Vitamin C Molecules in Liposome-Based Drug Delivery Systems: An In Silico Study, *Adv. Pharmacol. Pharm. Sci.*, 2023, **2023**, 4301310.
54 C. Tan, J. Xue, X. Lou, S. Abbas, Y. Guan, B. Feng, X. Zhang and S. Xia, Liposomes as delivery systems for carotenoids: Comparative studies of loading ability, storage stability and in vitro release, *Food Funct.*, 2014, **5**, 1232–1240.
55 C. Tan, B. Feng, X. Zhang, W. Xia and S. Xia, Biopolymer-coated liposomes by electrostatic adsorption of chitosan (chitosomes) as novel delivery systems for carotenoids, *Food Hydrocolloids*, 2016, **52**, 774–784.
56 Y. Liu and Y. Liu, Construction of lipid-biomacromolecular compounds for loading and delivery of carotenoids: Preparation methods, structural properties, and absorption-enhancing mechanisms, *Crit. Rev. Food Sci. Nutr.*, 2022, 1–24, DOI: **10.1080/10408398.2022.2118229**.
57 Y. Ben-Fadhel, B. Maherani, S. Salmieri and M. Lacroix, Preparation and characterization of natural extracts-loaded food grade nanoliposomes, *LWT*, 2022, **154**, 112781.
58 M. Hasan, G. B. Messaoud, F. Michaux, A. Tamayol, C. J. F. Kahn, N. Belhaj, M. Linder and E. Arab-Tehrany, Chitosan-coated liposomes encapsulating curcumin: study of lipid–polysaccharide interactions and nanovesicle behavior, *RSC Adv.*, 2016, **6**, 45290–45304.
59 L. Hou, X. Sun, L. Pan and K. Gu, Effects of Phytosterol Butyrate Ester on the Characteristics of Soybean Phosphatidylcholine Liposomes, *J. Oleo Sci.*, 2021, **70**, 1295–1306.

60 Y. Wei, C. Sun, L. Dai, X. Zhan and Y. Gao, Structure, physicochemical stability and in vitro simulated gastrointestinal digestion properties of β-carotene loaded zein-propylene glycol alginate composite nanoparticles fabricated by emulsification-evaporation method, *Food Hydrocolloids*, 2018, **81**, 149–158.

61 H. Rostamabadi, A. S. Mahoonak, A. Allafchian and M. Ghorbani, Fabrication of β-carotene loaded glucuronoxylan-based nanostructures through electrohydrodynamic processing, *Int. J. Biol. Macromol.*, 2019, **139**, 773–784.

62 M. Veverka, T. Dubaj, J. Gallovič, V. Jorík, E. Veverková, M. Mičušík and P. Šimon, Beta-glucan complexes with selected nutraceuticals: Synthesis, characterization, and stability, *J. Funct. Foods*, 2014, **8**, 309–318.

63 A. Shah, A. Gani, F. Masoodi, S. M. Wani and B. A. Ashwar, Structural, rheological and nutraceutical potential of β-glucan from barley and oat, *Bioact. Carbohydr. Diet. Fibre*, 2017, **10**, 10–16.

64 A. E. Kaziem, L. Yang, Y. Lin, H. Xu and Z. Zhang, β-Glucan-Functionalized Mesoporous Silica Nanoparticles for Smart Control of Fungicide Release and Translocation in Plants, *ACS Omega*, 2022, **7**, 14807–14819.

65 Z. u. Ashraf, A. Shah, A. Gani, F. A. Masoodi and N. Noor, Effect of nano-reduction on properties of β-glucan and its use as encapsulating agent for release of α-tocopherol, *Bioact. Carbohydr. Diet. Fibre*, 2020, **24**, 100230.

66 Y. Wu, W. Wang, Z. Yu, K. Yang, Z. Huang, Z. Chen, X. Yan, H. Hu and Z. Wang, Mushroom-brush transitional conformation of mucus-inert PEG coating improves co-delivery of oral liposome for intestinal metaplasia therapy, *Biomater. Adv.*, 2022, **136**, 212798.

67 Q. Lin, R. Liang, P. A. Williams and F. Zhong, Factors affecting the bioaccessibility of β-carotene in lipid-based microcapsules: Digestive conditions, the composition, structure and physical state of microcapsules, *Food Hydrocolloids*, 2018, **77**, 187–203.

68 J. D. Beltrán, C. E. Sandoval-Cuellar, K. Bauer and M. X. Quintanilla-Carvajal, *In vitro* digestion of high-oleic palm oil nanoliposomes prepared with unpurified soy lecithin: Physical stability and nano-liposome digestibility, *Colloids Surf., A*, 2019, **578**, 123603.

69 Y. Ji, Z. Wang, X. Ju, F. Deng, F. Yang and R. He, Co–encapsulation of rutinoside and β–carotene in liposomes modified by rhamnolipid: Antioxidant activity, antibacterial activity, storage stability, and in vitro gastrointestinal digestion, *J. Food Sci.*, 2023, **88**, 2064–2077.

70 Y. Ma, J. Xu, S. Jiang and M. Zeng, Effect of chitosan coating on the properties of nanoliposomes loaded with oyster protein hydrolysates: Stability during spray-drying and freeze-drying, *Food Chem.*, 2022, **385**, 132603.

71 J. Li, Y. Zhou, J. Zhang, L. Cui, H. Lu, Y. Zhu, Y. Zhao, S. Fan and X. Xiao, Barley β-glucan inhibits digestion of soybean oil in vitro and lipid-lowering effects of digested products in cell co-culture model, *Food Res. Int.*, 2023, **164**, 112378.

72 J. Yi, F. Zhong, Y. Zhang, W. Yokoyama and L. Zhao, Effects of lipids on in vitro release and cellular uptake of β-carotene in nanoemulsion-based delivery systems, *J. Agric. Food Chem.*, 2015, **63**, 10831–10837.

73 M. Nooshkam and M. Varidi, Physicochemical stability and gastrointestinal fate of β-carotene-loaded oil-in-water emulsions stabilized by whey protein isolate-low acyl gellan gum conjugates, *Food Chem.*, 2021, **347**, 129079.

74 H. Liu, X. Zeng, J. Huang, X. Yuan, Q. Wang and L. Ma, Dietary fiber extracted from pomelo fruitlets promotes intestinal functions, both in vitro and in vivo, *Carbohydr. Polym.*, 2021, **252**, 117186.

75 A. Mackie, N. Rigby, P. Harvey and B. Bajka, Increasing dietary oat fibre decreases the permeability of intestinal mucus, *J. Funct. Foods*, 2016, **26**, 418–427.

76 J. Grießinger, S. Dünnhaupt, B. Cattoz, P. Griffiths, S. Oh, S. B. i Gómez, M. Wilcox, J. Pearson, M. Gumbleton and M. Abdulkarim, Methods to determine the interactions of micro-and nanoparticles with mucus, *Eur. J. Pharm. Biopharm.*, 2015, **96**, 464–476.

77 M. Valibeknejad, S. M. Abdoli, R. Alizadeh, S. M. Mihăilă and A. Raoof, Insights into transport in mucus barrier: Exploring particle penetration through the intestinal mucus layer, *J. Drug Delivery Sci. Technol.*, 2023, **86**, 104752.

78 S. Bhattacharjee, E. Mahon, S. M. Harrison, J. McGetrick, M. Muniyappa, S. D. Carrington and D. J. Brayden, Nanoparticle passage through porcine jejunal mucus: Microfluidics and rheology, *Nanomedicine*, 2017, **13**, 863–873.

79 V. Puri, V. P. Kaur, A. Singh and C. Singh, Recent advances on drug delivery applications of mucopenetrative/mucoadhesive particles: A review, *J. Drug Delivery Sci. Technol.*, 2022, 103712.

80 S. P. Bandi, Y. S. Kumbhar and V. V. K. Venuganti, Effect of particle size and surface charge of nanoparticles in penetration through intestinal mucus barrier, *J. Nanopart. Res.*, 2020, **22**, 1–11.

81 C. S. Schneider, Q. Xu, N. J. Boylan, J. Chisholm, B. C. Tang, B. S. Schuster, A. Henning, L. M. Ensign, E. Lee, P. Adstamongkonkul, B. W. Simons, S.-Y. S. Wang, X. Gong, T. Yu, M. P. Boyle, J. S. Suk and J. Hanes, Nanoparticles that do not adhere to mucus provide uniform and long-lasting drug delivery to airways following inhalation, *Sci. Adv.*, 2017, **3**, e1601556.

82 R. Pangeni, T. Meng, S. Poudel, D. Sharma, H. Hutsell, J. Ma, B. K. Rubin, W. Longest, M. Hindle and Q. Xu, Airway mucus in pulmonary diseases: Muco-adhesive and muco-penetrating particles to overcome the airway mucus barriers, *Int. J. Pharm.*, 2023, **634**, 122661.

83 M. Garcia-Diaz, D. Birch, F. Wan and H. M. Nielsen, The role of mucus as an invisible cloak to transepithelial drug delivery by nanoparticles, *Adv. Drug Delivery Rev.*, 2018, **124**, 107–124.

84 M. Zhang, J. A. Kim and A. Y.-C. Huang, Optimizing tumor microenvironment for cancer immunotherapy: β-glucan-based nanoparticles, *Front. Immunol.*, 2018, **9**, 341.

85 A. Rieder, S. H. Knutsen, A. S. Fernandez and S. Ballance, At a high dose even partially degraded beta-glucan with decreased solubility significantly reduced the glycaemic response to bread, *Food Funct.*, 2019, **10**, 1529–1539.

86 L. Chen, W. Yokoyama, P. Alves, Y. Tan, J. Pan and F. Zhong, Effect of encapsulation on β-carotene absorption and metabolism in mice, *Food Hydrocolloids*, 2021, **121**, 107009.